

Impurity lattice location in ion-implanted beryllium: Measurements and systematics

R. Vianden,* E. N. Kaufmann, and J. W. Rodgers

Bell Laboratories, Murray Hill, New Jersey 07974

(Received 23 January 1980)

As part of a program to examine the ion implantation process in metals, the lattice location of 24 elements implanted into beryllium has been studied using the ion-beam channeling technique. A qualitative inspection of the data showed that the major fraction of all implants, except H and He, occupy a highly unique site in the vicinity of either the substitutional, the tetrahedral interstitial, or the octahedral interstitial position in the Be lattice. Quantitative comparisons of the data were made with the results of analytical calculations in the continuum model of the channeling process as well as with the results of a Monte Carlo computer simulation using the binary collision model. Classical metallurgical parameterizations, such as Darken-Gurry plots fail to adequately account for observed impurity site preference. Elemental parameters devised by Miedema have however been successful in relating choice of lattice site to the properties of the impurity relative to those of Be.

I. INTRODUCTION

Ion implantation is now a well-established technique for the introduction of impurities into the near-surface region of materials. It is currently used to inject dopants in the manufacture of semiconductor devices and is finding application in the area of metals and alloys as well.¹ One major advantage of this technique is its ability to provide an "alloy" between constituents without regard to their chemical or metallurgical compatibility. Thus obstacles to thermal diffusion or alloying in the melt such as solubility limits or chemical reactivity can be avoided. For this reason, alloy systems created by implantation will be metastable, in general, and little guidance can be expected from the equilibrium binary phase diagram with regard to the physical state of such a system. It is already known that at relatively high impurity concentrations one might obtain metastable solid solutions, amorphous or disordered structures, or intermetallic compounds, for example.²

From a fundamental viewpoint and, to the extent that concentrated alloy properties are related to those of the dilute case, also from a practical viewpoint, it would be desirable to develop an understanding of the factors which determine the isolated impurity-host configuration achieved by implantation. This is a complex problem and certainly involves both the chemistry of the elements and the ballistic effects, such as lattice defects, attendant to the implantation process itself. Two rather different and somewhat complementary methods have been applied to the study of the microscopic disposition of implanted impurities. From hyperfine-interaction measurements, which yield values for the electromagnetic fields im-

posed on an impurity by its surroundings, one can infer site symmetries, defect trappings, etc. Ion beam channeling on the other hand can determine more directly where, with respect to the lattice of the host, the impurity is situated. Channeling measurements have been performed on a wide variety of dilute implanted systems and results have been summarized by Picraux.³ Combining data of hyperfine-interactions and channeling studies to characterize an implant has been discussed by deWaard and Feldman⁴ who also attempted to systematize lattice location results. Aside from the light metalloid impurities such as B or C, most impurities were found to be either substitutional (on a regular lattice site), in an apparently random location (presumably defect associated), or a combination of these.

By displaying data for an Fe host on a conventional Darken-Gurry plot⁵ which locates elements according to electronegativity and atomic size, deWaard and Feldman² showed that substitutional implanted elements were found grouped around the Fe point. This indicated a similarity between criteria, such as the Hume-Rothery⁶ rules, for solid solubility⁷ and those which would determine implant substitutionality. In fact, judging from available data, solubility is a sufficient condition to insure substitutionality on implantation but is not necessary since there are several examples of insoluble elements occupying regular lattice sites after implantation. To account for the latter observation, Sood and Dearnaley⁸ have relaxed the Hume-Rothery limits so that they apply to the implanted alloy. Notwithstanding this progress, the understanding of the implantation process is still rather rudimentary and can be summarized as follows. If an implanted element differs substantially

from the host in electronegativity and/or size, the impurity atom will trap or be trapped by native defects or more likely by those arising from the radiation damage accompanying its slowing down (collision cascade) in the host lattice. Impurities more similar to the host will be less attractive to defects and will favor substitutional sites. The concentration of substitutional impurity may exceed solubility limits because the process of slowing down and stopping of an ion is analogous to a rapid quench where high-energy configurations may be retained and because in most systems there is a substantial probability that the impurity will come to rest by undergoing a ballistic replacement collision with a host atom. The detailed interplay of metallurgical and ballistic effects must depend on the particular elements involved as well as on parameters such as temperature. We believe that the channeling results obtained for a Be host, which are reported below, provide the first clear opportunity to study the metallurgical aspects of the implantation mechanism without the additional complexities of ballistic effects. After presenting the experimental details, results, and analysis in Secs. II–IV, we will offer justification for this view in Sec. V where the results are systematized and explained in terms of metallurgical parameters.

Interest in Be arose from its use as a convenient hexagonal-close-packed host for hyperfine-interaction studies. Channeling measurements⁹ which were needed to interpret these studies for Ag, Cd, and In implantation showed a substitutional site (Ag) as well as an unprecedented unique tetrahedral interstitial site (Cd, In). Further measurements, also related to hyperfine-interactions work, showed that Pd,¹⁰ Hf,¹⁰ Hg,¹¹ and Au (Ref. 12) resided on substitutional, tetrahedral, octahedral-like, and substitutional sites, respectively. The unique nature of these early results motivated the systematic study of the implanted impurity lattice location in Be for several additional cases which is reported here in detail. Some aspects of the work for the impurities Os,¹³ Zn,¹⁴ Ga, W, Tl, Pb, and Bi,¹⁵ and Li (Ref. 16) have been previously communicated and a letter¹⁷ describing observed systematics has already appeared.

II. MEASUREMENT TECHNIQUE AND EXPERIMENTAL DETAILS

The ion-beam channeling technique was employed to determine the lattice sites of the various implanted elements.¹⁸ The yield of processes which require small impact parameter collisions between the incident ion and a host or impurity atom (e.g., wide-angle Rutherford scattering, nuclear reactions, inner-shell x-ray production) is recorded as a function of the angle between a major crystal-symmetry direction and the incident ion beam (angular scan). The lattice

location of the implanted atoms can then be derived from comparisons of host and impurity yield variations for angular scans of several crystal directions (triangulation).

In most cases presented here, Rutherford scattered $^4\text{He}^+$ ions from host and impurity atoms were observed. The low mass of Be ($A = 9$) ensures that the Be host continuum and the impurity peak in the energy spectrum of the backscattered ions are well separated. The spectral feature corresponding to the ions backscattered from the impurity is a peak because the implanted impurity atoms reside in a buried layer at a certain depth below the surface of the host material. For the lattice location of the light impurities, H, He, Li, and B, the detection of nuclear-reaction products served as a signature of collisions between the incident ions and the impurity.

A. Sample preparation

The beryllium single crystals used in these experiments were cut from a crystal boule obtained from the Franklin Institute Research Laboratories.¹⁹ After determination of the crystal orientation from Laue back-reflection x-ray analysis, small plates were spark cut under oil. Surface damage from the cutting process was removed by mechanical polishing and subsequent etching. The final size of the single crystals was approximately $15 \times 5 \times 1 \text{ mm}^3$. The orientation of the major crystal directions, for the samples most frequently employed was such that the normal to the largest sample face lay in the (0001) plane midway between the $\langle 10\bar{1}0 \rangle$ and $\langle 11\bar{2}0 \rangle$ axes. The stereogram appropriate for channeling in the hcp crystal with this orientation can be found in Ref. 15. In a few cases crystals cut parallel to the basal plane were also used.

A Rutherford backscattering analysis of the unimplanted crystals showed C and O as major surface impurities and Ni as the only observable bulk impurity, with an estimated bulk concentration of 20 at. ppm. Excess Ni had a tendency to remain at the crystal surface after the etching process. The resulting Ni peak (corresponding to about $\frac{1}{3}$ of a monolayer) in the energy spectrum interfered with the foreign atom location measurements if the mass of the foreign atom was in the $A = 60$ region.

Electromagnetic isotope separators (Ortec, $V_{\text{max}} = 300 \text{ kV}$ or Lintott, $V_{\text{max}} = 80 \text{ kV}$) were used to implant the various species of foreign atoms into the Be crystals. In order to avoid channeling effects during the implantation, the single crystals were tilted to avoid alignment of major symmetry directions with the beam. All implants were carried out at room temperature. Typical ion energies were 100 keV and doses lay in the 10^{14} ions/cm² range. In a few cases, due to the above mentioned Ni surface impurity, ion

TABLE I. Implantation parameters and final site assignments for impurities localized in beryllium.

Implanted element	Ion energy (keV)	Dose (10^{14} at./cm ²)	Range (Å)	Straggling (Å)	Estimated peak vol. concentration (at. ppm)	Site expt. result
H	13,10,7 ($\frac{1}{3}$ of total dose at each energy)	50 (total)	1780–1080	± 263 –207	2500	near basal plane
He	12,10,8 ($\frac{1}{3}$ of total dose at each energy)	50 (total)	960–625	± 200 –160	2500	random
Li	30,24,18,12 ($\frac{1}{4}$ of total dose of each energy)	100 (total)	1630–680	± 220 –160	4000	substitutional
B	16,12,8 ($\frac{1}{3}$ of total dose at each energy)	50,40, and 10 in different runs	510–260	± 150 –80	6600,5300 1300	random and substitutional (sample dependent)
Ne	25,15 ($\frac{1}{2}$ of total dose at each energy)	10	400–240	± 130 –75	2100	not determined—but definite interstitial component
Al	40	5	485	± 140	1100	not determined—but definite interstitial component
Ti	200	4	1700	± 330	400	tetrahedral
V	200	4	1700	± 330	400	tetrahedral
Ga	200	3	1140	± 220	500	octahedral-like
Ge	50	2.5	320	± 65	1200	octahedral-like
As	50	2.5	320	± 65	1200	octahedral-like
Mo	70	3	390	± 70	1400	tetrahedral
Sb	100	2.5	480	± 80	1000	octahedral-like
I	100	2	460	± 75	900	octahedral-like
Xe	100	2	460	± 75	900	octahedral-like
Cs	100	2	460	± 75	900	octahedral-like
Ba	100	2	460	± 75	900	octahedral-like
Gd	100	2	450	± 65	1000	tetrahedral
Ta	100	1	440	± 65	500	tetrahedral
W	100	1	440	± 65	500	tetrahedral
Os	100	1	440	± 65	500	substitutional
Pt	100	1	435	± 60	500	substitutional
Tl	100	1	430	± 55	600	octahedral-like
Pb	100	1	430	± 55	600	octahedral-like
Bi	100	1	430	± 55	600	octahedral-like
Th	50	1	280	± 35	950	tetrahedral
U	50	1	280	± 35	950	tetrahedral

energies were adjusted so that the depth of the implanted layer was such as to provide a clear separation from the Ni peak in the energy spectrum. For the lower Z elements, the doses were increased in order to compensate the effect of the Z^2 dependence of the Rutherford scattering cross section. All implantation parameters are collected in Table I, where range, straggling, and peak volume concentrations based on Schiott²⁰ are also given. Information on metallurgical solubility in beryllium for the elements studied here is either not available or negative²¹⁻²⁶ with the exception of Au which is known to be soluble.²⁷

B. Experimental arrangement

The 2 MV Van de Graff at Bell Laboratories was employed in all experiments. Usually a 1.9 MeV beam of $^4\text{He}^+$ collimated to a diameter of 1 mm and an angular divergence of $\pm 0.03^\circ$ was used. The Be crystals were mounted in a two-axis, computer-controlled goniometer, which was driven by stepping motors. The beam fluence for each point of an angular scan was measured by integration of the beam current on the samples, with secondary electrons suitably suppressed. In order to avoid surface contamination of the samples during the measurements, the sample holder was surrounded by a shield cooled to liquid-nitrogen temperature with ports for the incident beam and detectors. The pressure in the target chamber was typically 1×10^{-6} Torr.

The backscattered ions were detected in a 300 mm² annular Si-surface-barrier detector at 180° . The 1.9 MeV $^4\text{He}^+$ ions backscattered at 180° from Be have a rather low energy and their signal is somewhat difficult to separate from detector noise. An additional small surface barrier detector at 120° was therefore used to monitor scattering from Be, where the energy of the scattered $^4\text{He}^+$ is 1.6 times greater than at 180° , and is sufficient to separate their signal from the noise. In all measurements, a pile-up rejection system described in Ref. 28 was employed.

A typical energy spectrum of the ions backscattered at 180° is shown in Fig. 1. Digital windows were set in the energy spectra about regions corresponding to ions scattered from the Be host and the implanted element. In addition, a window was set on a pulser peak in the 180° spectrum (Fig. 1). This was generated by a single channel analyzer set on the Be signal in the 120° detector in such a way as to select events corresponding to scattering from Be at the depth of the implanted layer. The count rate in these windows was integrated in a PDP 11/20 computer which, after a preset amount of beam current was collected on the sample, advanced the crystal to the next position of the angular scan. Typically scans of the (0001), (11 $\bar{2}$ 0), (10 $\bar{1}$ 0) planes and the $\langle 11\bar{2}0 \rangle$ and $\langle 10\bar{1}0 \rangle$ axes were recorded in each lattice location measurement.

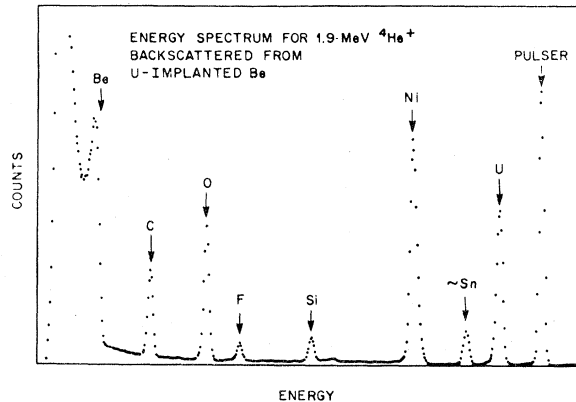


FIG. 1. Typical energy spectrum of $^4\text{He}^+$ backscattered from uranium-implanted beryllium. Note the surface impurities due to vacuum pump oil, C, Si, surface oxidation O, and the etching process F. Ni is a bulk impurity which is removed in the sample etching process along with Be and apparently is chemically plated back on the sample to the extent of $\sim \frac{1}{3}$ monolayer. The origin of the impurity with mass in the Sn region is not known and was not present on most samples.

III. EXPERIMENTAL RESULTS

Pronounced structure in the angular scans for the yield of ions backscattered from the foreign atoms was observed for nearly all implants. According to their main features, the data could be grouped into three categories, which in turn could be associated preliminarily with impurity atom location in three different regions in the hcp-Be lattice; the octahedral cage, the tetrahedral cage, and the substitutional position (see Fig. 2). The following discussion will be organized according to these three groups, and those cases where only very weak or no structure was found are gathered in Sec. III D.

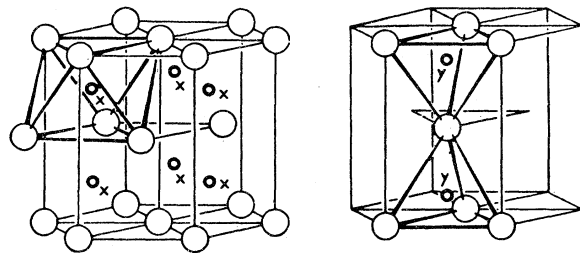


FIG. 2. Ideal interstitial sites in the close-packed hexagonal lattice. The ideal octahedral site (IOS) is labeled by x , the ideal tetrahedral site (ITS) by y . [After Hume-Rothery (Ref. 44).]

TABLE II. Experimental results for the half angular widths and minimum yields of the major crystal channels in the hcp-beryllium lattice. For comparison estimates based on empirical formulas given by Gemmel (Ref. 36) are included. For the unequally spaced $\langle 10\bar{1}0 \rangle$ plane no estimate could be calculated.

Channel	Experimental values		Empirical estimates	
	$\psi_{1/2}$	X_{\min}	$\psi_{1/2}$	X_{\min}
$\langle 11\bar{2}0 \rangle$	0.42°	0.06	0.52°	0.08
$\langle 10\bar{1}0 \rangle$	0.31°	0.14	0.40°	0.14
(0001)	0.17°	0.31	0.16°	0.32
$\langle 10\bar{1}0 \rangle$	0.23°	0.52		
$\langle 11\bar{2}0 \rangle$	0.19°	0.45	0.18°	0.51

Typical critical angles and minimum scattering yields characterizing the channeling effect in the Be host lattice, as obtained with a 1.9 MeV $^4\text{He}^+$ beam, are collected in Table II. After most implantations and after the lattice location measurements, no significant variations in the minimum yields were observed. This indicates that lattice damage caused by the implantation process and the analyzing beam did not materially affect the overall channeling quality of the crystals.

A. Substitutional cases

In a channeling experiment, a foreign atom which replaces a host-lattice atom will always see the same flux of incoming ions as seen by a nearby host atom. The variation of the yield of ions backscattered from substitutional foreign atoms and host atoms at approximately the same depth should therefore be identical for angular scans across all crystal directions. From crystal symmetry considerations, it can be concluded that an apparently substitutional result for a few crystal directions, e.g., the (0001) and the $\langle 11\bar{2}0 \rangle$, implies substitutionality of the element under consideration. Thus from the results for Au in Be (Fig. 3), it can be concluded that within the limits of error, 100% of the Au atoms reside on substitutional lattice sites after implantation. Including possible normalization errors, the uncertainty was estimated to be less than 5%.

Pt and Ni were also found to be totally substitutional. The lattice location of Ni was carried out with a small amount of Ni which was diffused (rather than implanted) from the previously mentioned Ni surface contamination into the Be-bulk material at a tempera-

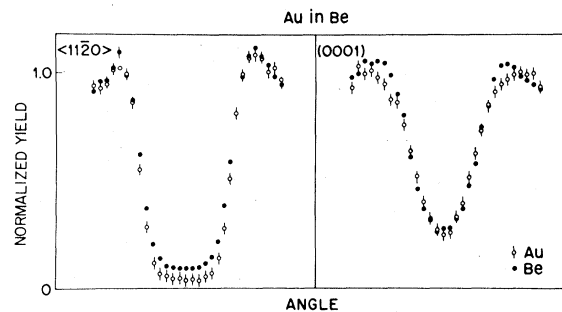


FIG. 3. Angular dependence of the normalized back-scattering yield of 1.9 MeV $^4\text{He}^+$ ions from Au implanted Be. Note that the high substitutionality of the Au and the extremely low-minimum yield for channeling in the $\langle 11\bar{2}0 \rangle$ axis have revealed a background contribution to the Be signal arising from the small amount of surface oxide and scattering from the Ni impurity from deep in the sample. In this uncorrected data the Au dip therefore appears deeper than the host dip itself.

ture of approximately 600 °C.

Additionally Li,¹⁶ Zn,¹⁴ Pd,¹⁰ and Ag⁹ are known to be substitutional after implantation into beryllium.

Finally, Os in Be should be included in this group. It was found¹³ to reside very close to a substitutional site. Scans of the (0001) plane and the $\langle 10\bar{1}0 \rangle$ axis however showed slightly narrower yield reduction patterns (dips) for the Os than for the host thus indicating a slight displacement of the Os atoms from an ideal substitutional position along the $\langle 0001 \rangle$ direction.

In some cases the Be single crystals were annealed for 30 min at several temperatures up to 600 °C in a vacuum of 2×10^{-6} Torr. After each annealing step the crystals were cooled to room temperature and angular scans across the major crystal directions were repeated. For the typical substitutional case of Au, the onset of diffusion was observed at 600 °C and the diffused Au was found to stay on substitutional sites. Therefore it can be concluded that not only in the metastable situation after implantation but also in thermal equilibrium, Au prefers the substitutional site in the Be lattice. This result is in agreement with the literature.^{22,27}

More surprisingly, a similar result was observed for Os in Be.¹³ The Os atoms also started to diffuse at 600 °C while staying in their displaced substitutional position. This, in analogy with the Au result, seems to indicate a finite solubility of Os in Be in contrast to metallurgical studies.²⁴

Pd in Be is also known to remain substitutional while diffusing in Be after implantation as could be concluded from hyperfine-interaction measurements described in Ref. 10.

B. Tetrahedral cases

For a large number of implants, the angular scans showed almost complete substitutional behavior for the $(11\bar{2}0)$ and $(10\bar{1}0)$ planes and a more or less pronounced double peak for the $\langle 11\bar{2}0 \rangle$ axis (see, e.g., Fig. 4 for Gd). This coupled with a narrowed impurity dip in the scan of the (0001) plane is in excellent qualitative agreement with the assumption that 100% of the implanted atoms reside on the tetrahedral interstitial site, as will be explained in more detail below. Generally similar results were obtained for Ti, V, Mo (Fig. 5), Ta, W, Th, and U. However a comparison of Figs. 4 and 5 shows small differences in the detailed structure of the impurity scans which indicate slight differences in the exact spatial positions of, e.g., Gd and Mo in the tetrahedral interstitial cage.

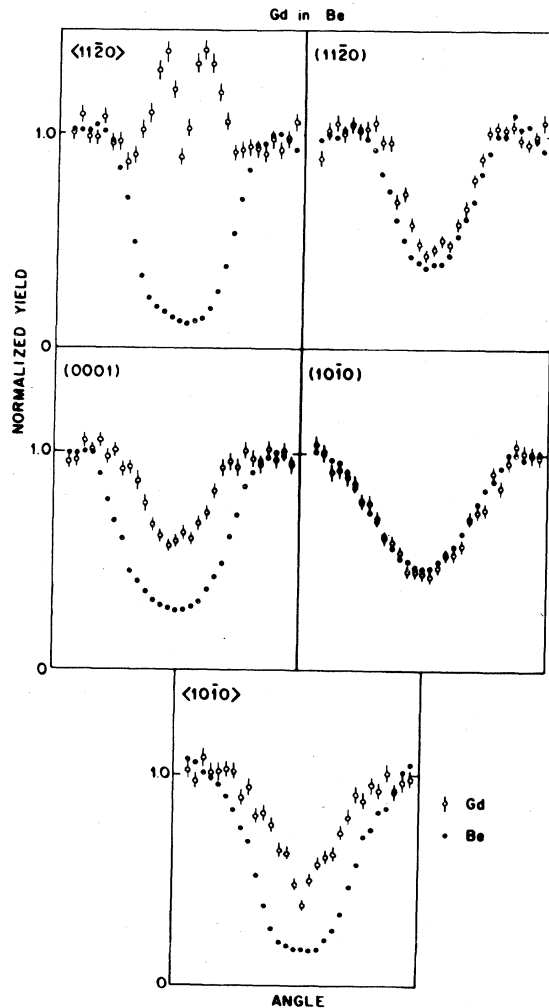


FIG. 4. Angular dependence of the normalized back-scattering yield of 1.9 MeV $^4\text{He}^+$ ions from Gd implanted Be.

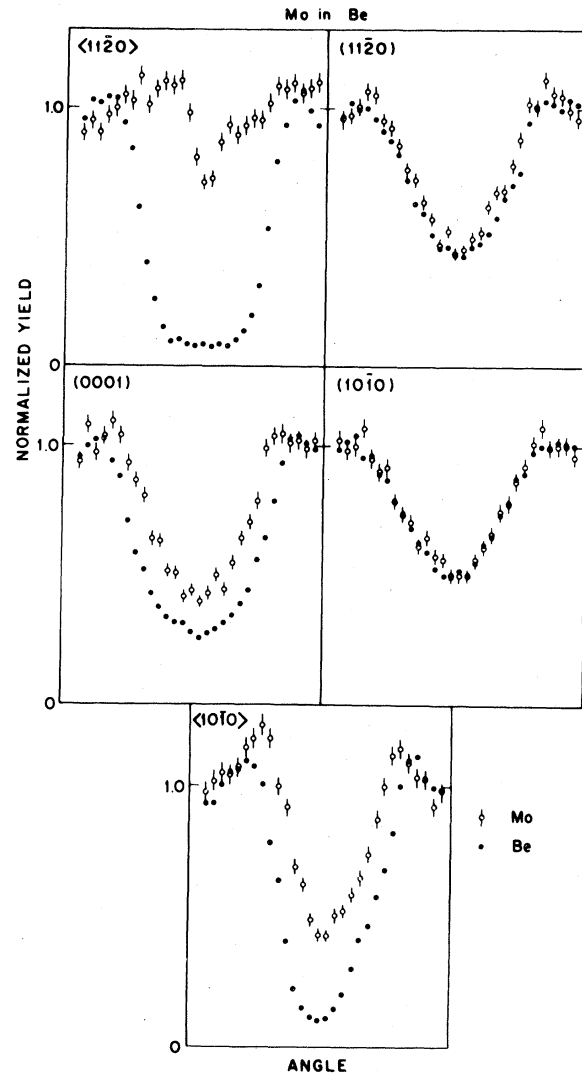


FIG. 5. Angular dependence of the normalized back-scattering yield of 1.9 MeV $^4\text{He}^+$ ions from Mo implanted Be.

Beside the elements just mentioned, Hf,¹⁰ In,⁹ and Cd (Ref. 29) are also known to occupy a tetrahedral-like site after implantation into Be. In these cases the annealing behavior of the implants was also studied. Channeling and hyperfine-interaction investigations^{10,29} showed that after annealing at approximately 400 °C, these elements either precipitate almost completely from the Be host or trap defects.

C. Octahedral cases

A third class of angular scans showed strong flux peaks for the impurity in the $\langle 11\bar{2}0 \rangle$, $\langle 10\bar{1}0 \rangle$, (0001) , and $(10\bar{1}0)$ channels (Figs. 6 and 7). Only along the $(11\bar{2}0)$ direction could a dip be observed, which was however in all cases considerably shallower

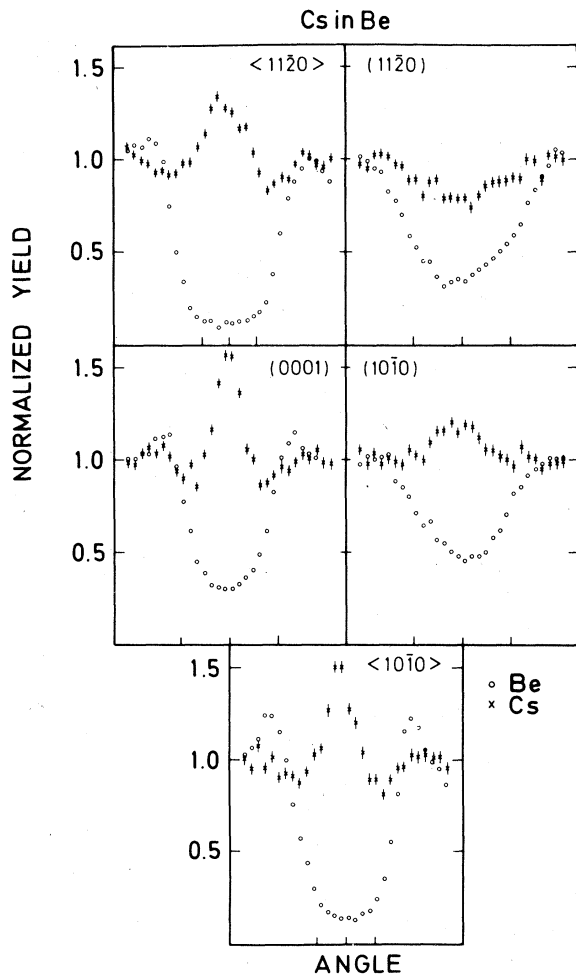


FIG. 6. Angular dependence of the normalized backscattering yield of 1.9 MeV $^4\text{He}^+$ ions from Cs implanted Be.

than the host dip. These structures are roughly consistent with the assumption of an ideal octahedral interstitial site for the implanted elements. Similar results were found for Ge, As, Sb, I, Xe, Cs, Ba, Tl, Pb, and Bi. For Ga in Be (Fig. 8), the strong flux peak in the $\langle 11\bar{2}0 \rangle$ is missing and the (0001) plane shows a narrow dip. That makes this case less conclusive, but seems to indicate a strongly-displaced octahedral site for the Ga atoms. A comparable situation was found for Hg in Be,¹¹ where a displaced-octahedral site was also inferred from the data.

For Bi the angular scans were repeated after annealing the Be crystal at various temperatures up to 600 °C. After annealing for 30 min at 300 °C, all structure in the angular scans disappeared, which indicated a highly nonunique (random) position of the Bi atoms in the Be host lattice, caused most probably by precipitation or defect trapping.

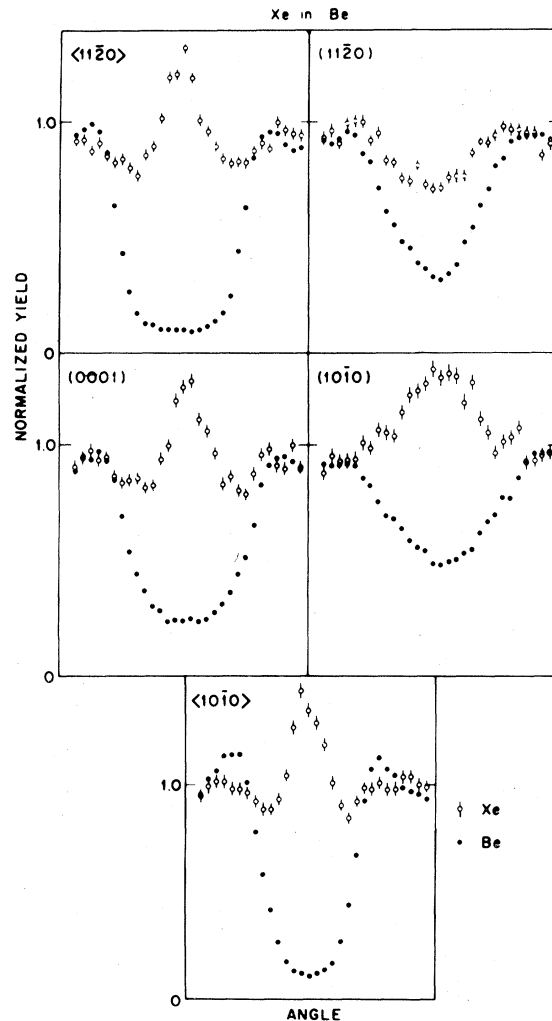


FIG. 7. Angular dependence of the normalized backscattering yield of 1.9 MeV $^4\text{He}^+$ ions from Xe implanted Be.

D. Low-mass impurities

In addition to Li which is mentioned in Sec. III A, other impurities of relatively low mass were studied. In particular ^2H (deuterium), ^3He , ^{10}B , ^{20}Ne , and ^{27}Al were investigated^{30,31} using nuclear reaction techniques for H and ^3He , Rutherford backscattering for ^{20}Ne and ^{27}Al , and both methods for ^{10}B . Unlike the result for Li, which was unambiguously substitutional, no definitive site assignment could be deduced for the other cases. In all instances, counting rates were low and the amount of data correspondingly limited. For ^2H , ^3He , and ^{10}B , angular scans were obtained for some channeling directions, but for ^{20}Ne and ^{27}Al only yields for random incidence and for perfect

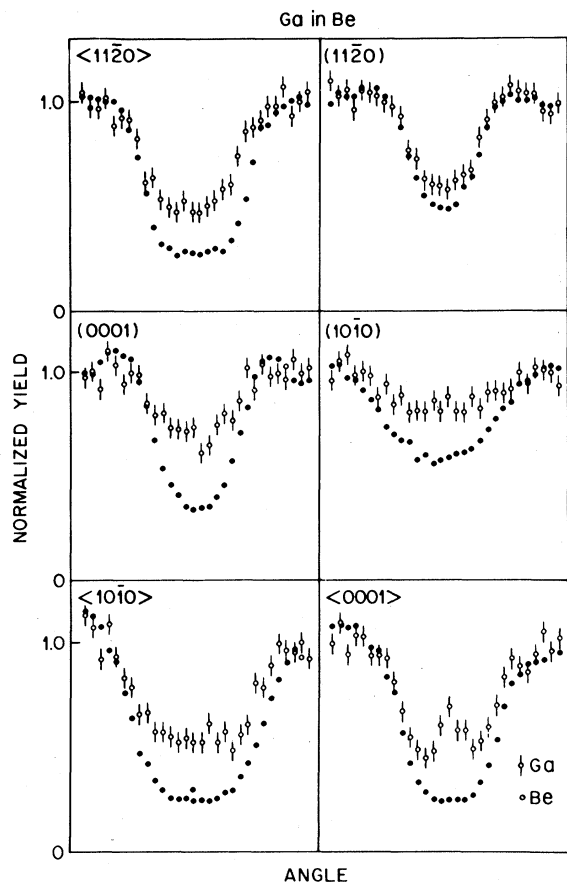


FIG. 8. Angular dependence of the normalized backscattering yield of 1.9 MeV $^4\text{He}^+$ ions from Ga implanted Be.

alignment with a channel could be compared. In order to achieve even this, an order of magnitude ($1 \times 10^{15} / \text{cm}^2$) or more implanted dose was necessary which may take us out of the dilute alloy regime.

For ^2H , occupancy of sites near the basal planes of atoms could be inferred from scans of the (0001) plane but no single site of high symmetry within the plane could be deduced from additional data. Even less definitive results for ^3He were found where for all channeling directions only small deviations from a random reaction yield could be seen. Both results may be indicative of the strong influence of lattice defects. Supporting this hypothesis is the observation that changes in the results occurred at high analyzing beam fluence, thus necessitating moving of the beam spot to fresh areas of the samples.

^{10}B appears $\sim 60\%$ substitutional plus 40% random for experiments performed on the usual " \hat{a} -cut" Be crystals, whereas it appears $\sim 100\%$ random in the " \hat{c} -cut" samples. This result is verified for both Rutherford-backscattering and nuclear-reaction modes of observation and for low ($1 \times 10^{15} / \text{cm}^2$) as

well as high ($5 \times 10^{15} / \text{cm}^2$) boron doses. This may point to an anisotropy in the susceptibility of Be to radiation damage, with a large damage cross section for incidence near the $\langle 0001 \rangle$ axis. Without additional confirmation of this hypothesis and in view of the discrepancy between different samples, this case is omitted from the substitutional category of Sec. III A.

For ^{20}Ne and ^{27}Al , it can only be stated with certainty that some fraction of each occupies a rather unique and probably different nonsubstitutional site. Apparent substitutional fractions at perfect alignment varied from 0 to $>80\%$ depending on the channeling direction but not in a way which conclusively pointed to the tetrahedral or octahedral sites. In addition there may be random and substitutional components in both cases with combined populations as high as 50%.

It is important to note that no such severe ambiguities arise in the classification of results for other impurities which are more massive relative to Be and for which lower dose implants were possible. A plausible justification for this state of affairs is offered in Sec. V where the special case of the Li impurity is discussed.

IV. INTERPRETATION OF CHANNELING RESULTS

For a quantitative interpretation of the lattice location data of nonsubstitutional implants, it is necessary to have a detailed knowledge of the ion-flux distribution in each channel as a function of the angle ϕ between beam and channel and of the distance beneath the crystal surface. Since this flux distribution is influenced by various parameters such as divergence of the incident beam, surface damage, or oxide layers on the crystal, thermal vibrations of the host atoms as well as collisions of the channeling ions with the electrons of the solid, this information is extremely difficult to obtain. However if one makes some theoretical simplifications, it is often possible to get a rough idea of the flux variation with ϕ at a given position in a channel. In the following, the various steps of approximation to the real situation, used in the interpretation of the data, will be discussed.

A. Qualitative analysis

The simplest way to interpret the main features of the lattice location data, which was already used to group the experimental results in Sec. III, is to take the "particles eye view." Figure 9 shows schematically where an ion, channeling down one of the various major crystal directions, would see atoms of an element occupying the ideal tetrahedral (ITS) or octahedral (IOS) interstitial site. Knowing further that the guiding effect of the regularly arranged crystal

FAVORED INTERSTITIES IN HCP LATTICE
(PROJECTED ON PLANE NORMAL TO INDICATED CHANNEL)

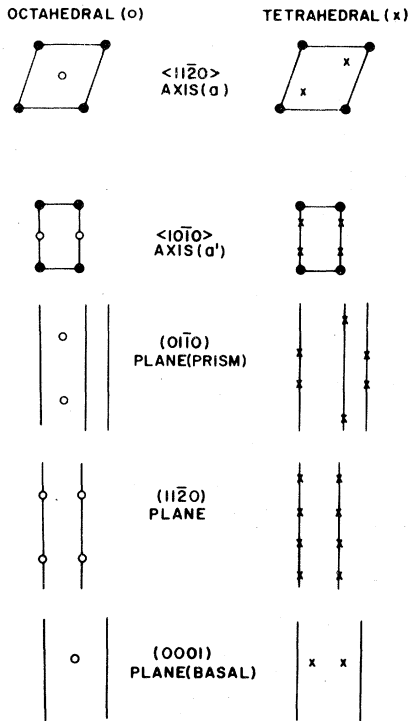


FIG. 9. Projections of the ideal tetrahedral (ITS) and ideal octahedral sites (IOS) in a hcp lattice on planes normal to the indicated channels.

atoms always steers the ions towards the center of the channel, one expects an increased flux in the center channel region (flux peaking). Thus the number of ions backscattered from a foreign atom located in the center of a channel will have a maximum for perfect alignment ($\phi = 0^\circ$) and will decrease with increasing ϕ as the flux distribution approaches the random value.

Such a variation of the yield was observed, e.g., for Xe in Be (Fig. 7) in angular scans of the $\langle 11\bar{2}0 \rangle$, (0001), and $\langle 10\bar{1}0 \rangle$ channels. Therefore it can be concluded that the Xe atoms are situated near the center of these channels. As Fig. 9 shows, this is consistent only with Xe being located in the vicinity of the ideal octahedral site. The flux peak observed in the $\langle 10\bar{1}0 \rangle$ direction is also in agreement with this location of the Xe atoms since for $\phi = 0^\circ$ one would expect an enhanced flux at the octahedral position caused by ions which diffuse between neighboring $\langle 10\bar{1}0 \rangle$ channels via the low-potential region in the center of the basal plane. For the $\langle 11\bar{2}0 \rangle$ planar channel one would expect a totally substitutional result, since here the ideal octahedral site appears in the walls of the channel. Experimentally only a $\sim 50\%$ dip is found, which however is in qualitative

agreement with the above interpretation. Thus the main features of the data can be understood only by assuming that the implanted Xe atoms come to rest near the ideal octahedral site in the hcp-Be host lattice. By similar arguments most of the elements mentioned in Sec. III C could be located near the ideal octahedral site. Only for Ga, as mentioned above, did a dip observed in the (0001) plane make the interpretation less straightforward. However from a flux peak found in the $\langle 10\bar{1}0 \rangle$ plane and from the results for the $\langle 0001 \rangle$ axial channel studied in this case, it was concluded that Ga is located in the octahedral cage strongly displaced along the $\langle 0001 \rangle$ direction towards the basal plane. A similar situation is known to occur for Hg in Be.¹¹

The other group of results for which Gd in Be (Fig. 4) is a good example shows practically a total substitutional behavior for the $\langle 10\bar{1}0 \rangle$ and $\langle 11\bar{2}0 \rangle$ channels. Lattice symmetry dictates that a nonsubstitutional element can produce this result only if the foreign atoms occupy sites near the ideal tetrahedral site (Fig. 9). A narrowed dip observed in the (0001) channel is also consistent with this interpretation since the ideal tetrahedral site lies near the walls of this channel, thus seeing no flux enhancement for $\phi = 0^\circ$. The occurrence of a double flux peak separated by a narrow valley at $\phi = 0^\circ$ in the $\langle 11\bar{2}0 \rangle$ axis is more difficult to understand in our simple model. But regarding the off center position where the ideal tetrahedral site appears in this axis (Fig. 9), it seems not to be in contradiction to our assumption. For the $\langle 10\bar{1}0 \rangle$ axis the ideal tetrahedral site appears like the ideal octahedral site in the walls of the axial channel (Fig. 9). However its position much closer to the host atom strings can explain the narrow dip observed in the experiments. For the other elements classified by similar arguments as tetrahedral (Sec. III B) all general features of the angular scans were the same.

The results of this qualitative interpretation for all cases studied are gathered in column 7 of Table I.

B. Analytical simulations

A more detailed prediction of the flux variation at a given interstitial site was tried by using the Lindhard continuum-model description of the channeling process.³² In this model it is assumed that the interaction of the channeling ion, moving fast and nearly parallel to the channel axis, with the rows of individual atoms surrounding that channel, can be described by representing the rows of atoms as a continuous potential string. Similarly crystal planes are described as potential sheets. This approximation makes it possible to obtain the total potential in which the ion moves simply by summing over all potential strings surrounding, e.g., an axial channel.

In Fig. 10 the results of such a summation for the $\langle 11\bar{2}0 \rangle$ and $\langle 10\bar{1}0 \rangle$ axes in the hcp-Be lattice are shown. Here the standard row potentials given by Lindhard³² were used and, in the summation, the influence of the 12 next-near-neighbor strings was also taken into account. The interesting split potential

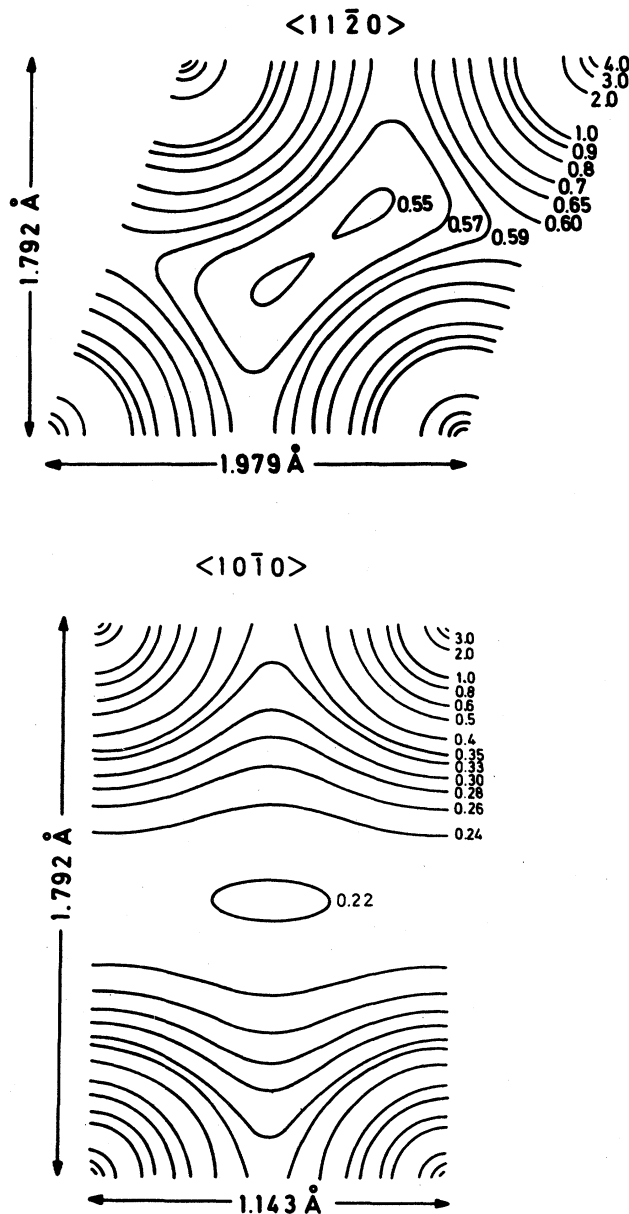


FIG. 10. Continuum potential maps for 1.9 MeV ${}^4\text{He}^+$ in hcp Be for the $\langle 11\bar{2}0 \rangle$ and $\langle 10\bar{1}0 \rangle$ axes. The 4 nearest- and the 12 next-nearest-atom strings were taken into account. Contours are labeled with the amplitude of the function $\ln(1 + 3a^2/|\bar{r} - \bar{r}_i|^2)$ summed over the 16 strings. In this function a is the Thomas-Fermi scattering distance and thermal vibrations are neglected.

minimum which appears in the $\langle 11\bar{2}0 \rangle$ axis is caused by the nonideal c/a ratio of the Be lattice.

Particles entering the channel will have a kinetic energy transverse to the channel axis determined by the potential at their point of entry and the incident angle ϕ . Then the region which an ion can sample is simply given by the condition that the potential has to be smaller than the transverse energy. If one now assumes that each particle can be found with equal probability in its accessible region (i.e., a statistical equilibrium has been reached), one can calculate the flux variation as a function of the angle of incidence for every point in the channel.

After adaptation to the hcp-Be lattice, a computer program based on these assumptions³³ was used to calculate yield variation as a function of entry angle for the experimentally investigated channels. As an example, the flux variation at the ideal tetrahedral site is shown in Fig. 11. From a comparison with the experimental results for Gd and Mo (Figs. 4 and 5) which are believed to occupy the ideal tetrahedral site, it can be seen that the main features are repro-

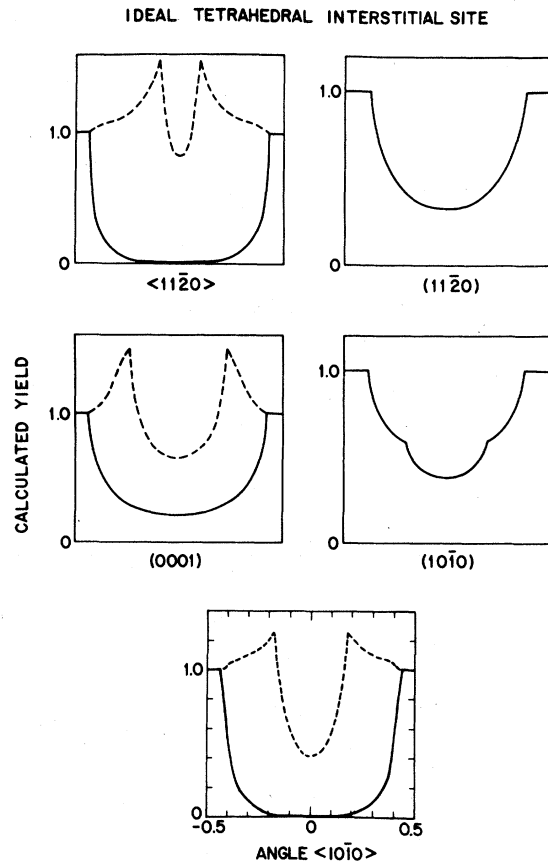


FIG. 11. Analytical simulation of the angular dependence of the backscattering yield of 1.9 MeV ${}^4\text{He}^+$ from Be (—) and an impurity (---) in the ideal tetrahedral site.

duced rather well. Although for the octahedral cases the agreement was less good, generally all site assignments made in Sec. IV A (see Table I) were confirmed.

However, it was found to be impossible to extract more detailed information on the spatial positions of the various implants from these simulations. The main reason is certainly that the assumption of a statistical equilibrium flux distribution is not fulfilled in the depth region where most of the implanted elements were situated. This can be concluded for example from the fact that angular scans through the same axial channel following different tilting planes resulted in slight changes in the structure of the yield curves. Further, for ${}^4\text{He}^+$ ions of similar energy channeling in the (0001) channel, Kaufmann³⁴ observed planar oscillations, a pronounced nonequilibrium effect.

Also the effects of electronic multiple scattering, thermal vibrations of the host atoms, and the finite beam divergence could not be easily incorporated in this analytical model. This and the fact that the predicted critical angle and minimum yield for all host scans is determined by a distance of closest approach parameter which seems to be inappropriate for the anisotropic Be lattice leads to poor agreement of the simulated host dips with the experimental results.

C. Binary collision model

In contrast to the previously discussed model, where the discrete structure of the crystal lattice was neglected, the guided motion of an ion through the crystal in reality is a series of collisions with the host atoms. In the binary collision model, each of these collisions is described as an isolated two-body collision, which can be treated classically. By solving the standard scattering integrals for every collision one can then derive the trajectory of an ion on its way through the channel. This was done by a computer simulation program, which by means of a Monte Carlo (MC) method generated random starting points of ions on the crystal surface. With a velocity equal to that in the experiment, the ions then moved into the crystal. In calculating the trajectories, the finite beam divergence, thermal vibrations of the host atoms, as well as small deflections of the ions caused by collisions with the electrons of the solid were taken into account. The position of an ion in a channel was monitored in regular depth intervals and thus after averaging over a sufficient number of ions (typically 625) and depth regions, a map of the ion flux distribution in a certain channel could be obtained. A detailed description of the basic structure of the program can be found in Refs. 33 and 35 although the capabilities of the program described there were extended to allow calculations in hexagonal-close-

packed lattices.

For the interaction potential between the charged particles and the host atoms the Moliere approximation to the Thomas-Fermi potential was employed. Using the expression given by Gemmel,³⁶ the Thomas-Fermi screening radius for fully ionized 1.9-MeV α particles in beryllium was derived to be 0.29 Å. The thermal vibrations of the host atoms were described in the Debye model assuming isotropic vibrations and a mean vibration amplitude of $|u| = 0.059 \text{ \AA} [T_{\text{Debye}}(\text{Be}) = 1440 \text{ K}]$.³⁷

Simulations were carried out for all crystal directions studied in the experiments. The tilting planes of the simulated scans were always kept very close to the experimental ones. The flux distribution in planes normal to the crystal direction under investigation was obtained by dividing an axial channel, for example, into a 20×20 rectangular grid and recording the number of ions passing through each grid square. Planar channels were analogously subdivided into 20 strips. Typically, the positions of 625 ions were then monitored every few angstroms along the particular crystal direction. Subsequently these flux distributions were averaged over the depth regions in which the implanted atoms came to rest in the beryllium host lattice. Thus flux distribution maps for the interesting depth intervals were obtained. As an example, the flux in the (0001) axis averaged over the interval from 270 to 550 Å for 0° angle of incidence is shown in Fig. 12.

For an assumed impurity site, angular yield variation curves could then be calculated by summing the flux through the grid squares which would be occupied by the impurity atom. The thermal vibration of the impurity atoms was approximated by a Gaussian-shaped isotropic probability distribution around the equilibrium site. The flux through the grid squares surrounding the equilibrium site was then weighted with the total probability to find the implanted atom in that square. Usually, the thermal vibration mean square amplitude of $u^2 = 0.00348 \text{ \AA}^2$ ($|u| = 0.059 \text{ \AA}$), which is equal to that of beryllium, was assumed.

Using the thus obtained flux maps for the 270 to 550 Å depth region, the simulated angular scans shown in Fig. 13 resulted. These correspond to an unique displaced tetrahedral site. Here quantitative agreement was sought with the experimental results for Mo in Be (Fig. 6) by displacing the impurity from the ITS toward the (0001) plane. Since the observed critical angle, $\phi_{1/2}$, for this plane is expected to be most sensitive to the amount of displacement, it was used to match the simulation to the experimental $\phi_{1/2}$ value. Discrepancies in minimum yield and shoulders had to be tolerated since these quantities depend strongly on surface oxide layers and imperfections in the crystal which were not determined experimentally. Furthermore, the thermal vibration amplitude of the impurity atom strongly influences the height of

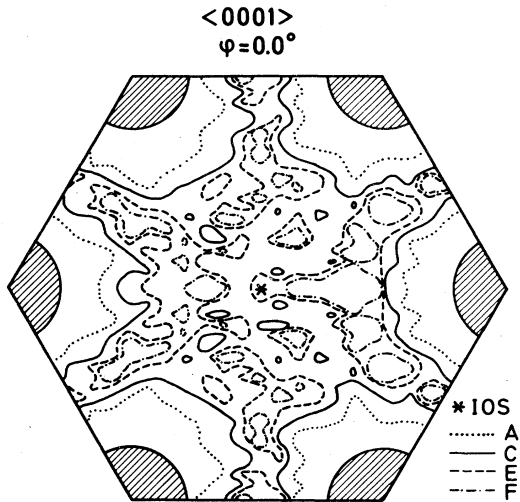


FIG. 12. Simulated flux distribution of 1.9 MeV α particles in the $\langle 0001 \rangle$ channel for $\phi = 0.0^\circ$ incidence averaged over the depth interval from 270 to 550 Å. The contour lines A, C, E, and F correspond to flux densities equal to 0.6, 1.0, 1.7, and 2.3 times the value for perfect random distribution. Note that the highest flux-density regions do not coincide with the potential minimum in the center of the channel (*) which means that a statistical equilibrium has not yet been reached. An impurity in the ideal octahedral site (IOS) would appear in the center of the channel. The shaded circle sections in the corners of the hexagon correspond to the Thomas-Fermi screening radius of the Be atoms for 1.9 MeV α particles.

the shoulders and the minimum yield. It is not certain that assuming an amplitude equal to that of beryllium is correct.

Thus for Mo in Be a position was derived which is 0.23 Å displaced from the ITS in the \hat{c} direction towards the basal plane. This impurity position led to simulated scans for the remaining crystal directions which were also in good agreement with the experimental results (Fig. 13).

Considering the narrow dip in the (0001) plane (Fig. 4), Gd in Be is obviously less displaced towards the walls of the (0001) channel than Mo. In this case best agreement with the experiment was obtained by assuming a 0.12 Å displacement of Gd in the same direction as Mo. However for Gd, the $\langle 11\bar{2}0 \rangle$ experimental result is less well reproduced (Fig. 13). This discrepancy can, in addition to the factors mentioned above, be attributed to differences in the scan direction between experiment and simulation. The scan directions in the experiments differed typically by about $\pm 5^\circ$.

In Fig. 14 the Monte Carlo simulation results for an impurity in the ideal octahedral site are shown. Again an impurity vibration amplitude equal to that of Be was used in the calculations. Here a compari-

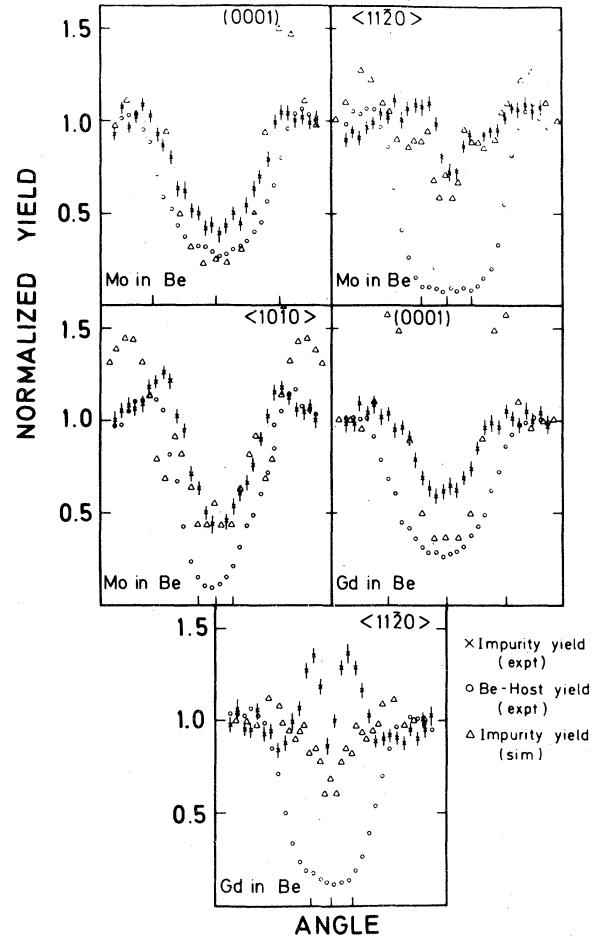


FIG. 13. Monte Carlo simulation of the angular dependence of the backscattering yield of 1.9 MeV $^4\text{He}^+$ from Mo and Gd in Be. For comparison the experimental results are included.

son with the experimental results for Cs and Xe (Figs. 6 and 7) shows an excellent qualitative agreement as far as position and width of flux peaks is concerned. Only in the case of the $\langle 10\bar{1}0 \rangle$ axis does the simulation lead to a scan with a central dip instead of a flux peak. A reason for this discrepancy could be that for this axis depth oscillations in the flux density cause a strong dependence of the scan shape on the impurity-depth distribution. To illustrate this, simulated axial scans for the depth interval 0–270 Å are shown in Fig. 14. Whereas for the $\langle 11\bar{2}0 \rangle$ the two scans are of an overall similar shape, for the $\langle 10\bar{1}0 \rangle$ a completely different scan shape is obtained. Thus slight deviations in the depth distribution of the implanted atoms from the values given in Table I could explain the disagreement.

Quantitatively the simulations lead to flux peaks which are about a factor of 2 too high. This is prob-

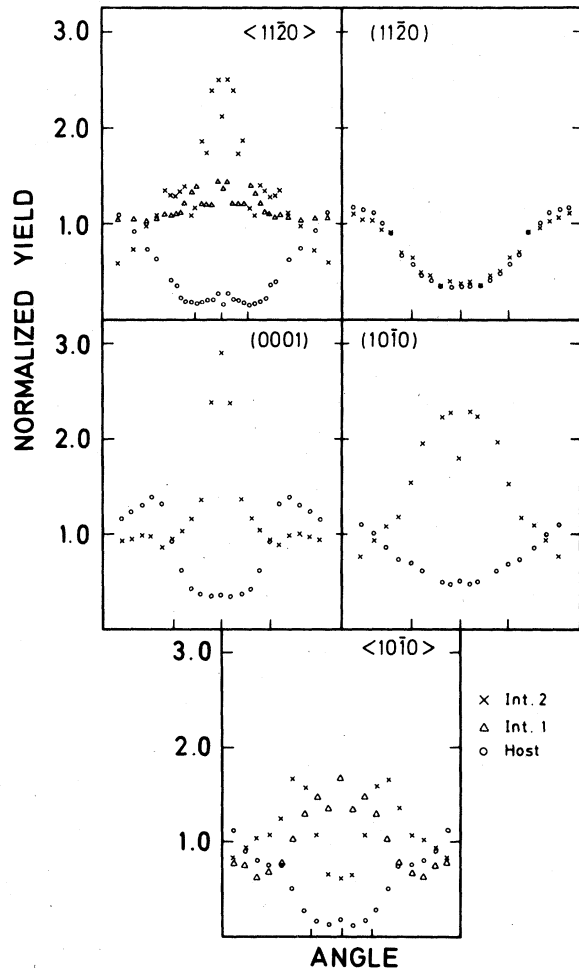


FIG. 14. Monte Carlo simulation of the angular dependence of the backscattering yield of 1.9 MeV $^4\text{He}^+$ from Cs in Be. Here, in addition to the 270–550 Å depth interval (Int. 2), results for the 0–270 Å interval (Int. 1) are included for the $\langle 11\bar{2}0 \rangle$ and $\langle 10\bar{1}0 \rangle$ axes.

ably due to the well-known³⁸ difficulty in MC simulations in reproducing with sufficient accuracy the path of the best channeled ions which determine the height of the central flux peaks. However, another possible explanation is suggested by the shallow impurity dip observed experimentally for the $(11\bar{2}0)$ plane, which for impurities uniquely in the IOS should show a totally substitutional result. If a large fraction of the implanted atoms come to rest on random (i.e., damage or BeO associated) sites, the height of flux peaks and the depth of impurities dips would be reduced. In order to obtain rough quantitative agreement one has to assume that approximately 70% of the impurity atoms occupy random lattice sites and only 30% are in the ideal octahedral site. There is not now adequate information to decide to

what extent limitations of the simulation or a randomly disposed impurity fraction accounts for the lack of quantitative agreement in these cases.

D. Summary of results

As a result of the analytical and Monte Carlo simulations, the qualitative site assignments of Sec. IV A were generally confirmed. For the impurities in the vicinity of the ideal tetrahedral site, the MC simulations led to a rather precise determination of the displacement from the ITS toward the basal plane. This together with the total substitutional result for the $(10\bar{1}0)$ and $(11\bar{2}0)$ planes, which excludes a displacement perpendicular to the \hat{c} axis, allows the derivation of the exact spatial position of the different implanted atom species.

In the case of the impurities in the octahedral cage, a similarly precise site determination was not possible. Here a conservative interpretation of the MC results would yield small fractions (typically 30%) of the implanted atoms on the IOS and a large fraction (70%) on random sites. However, a superposition of two or more different impurity sites could also lead to a good description of the data. Considering the remaining inaccuracies of the simulations, the results of such combined site models would not be convincing.

One principal difficulty in the interpretation is that the experimental channeling results only yield information about the position of an impurity species relative to the undisturbed host crystal. Thus local lattice relaxation around an impurity atom cannot be observed. Furthermore, the formation of well-defined and stable configurations between the impurity atom and host-lattice defects like interstitials or vacancies is possible. This effect has been observed by Swanson *et al.*³⁹ for Au in Zr and Ag in Mg, where the impurity atoms formed mixed dumbbells with host-lattice interstitials. In the case of the beryllium host, the formation of a Be-impurity dumbbell oriented in the \hat{c} -axis direction and with an impurity-dependent length could possibly explain the different displacements toward the (0001) plane for the impurities in the tetrahedral cage. It is also not possible to rule out a mixed dumbbell oriented in or near the (0001) plane as a configuration for impurities appearing to be in the octahedral interstice. In fact it is this type of dumbbell which Swanson *et al.*³⁹ actually infer from their data.

V. SYSTEMATICS

Questions still remain concerning the precise coordination of each implanted impurity atom with surrounding Be neighbors. Indeed, within the qualitatively distinguished categories of Secs. III B and III C, each set of data differed slightly, one from the other.

In order to characterize each result in detail, not only would a better quantitative data analysis method be required, but also the exact state of local lattice relaxation would need to be known. Then a complete quantum mechanical solution to the isolated impurity in Be problem (currently not a tractable problem) would be needed for each case to understand the results from the most fundamental viewpoint. This is certainly beyond present capabilities. Nevertheless, we have a substantial number of individual observations which taken together represent a good opportunity to search for a relationship between elemental properties and the implanted impurity state.

Systematic studies of the metallurgical site preferences of implanted atoms are usually hampered by two effects which are a natural byproduct of the implantation process itself. First the stopping of the impurity atom in the host lattice involves a series of nuclear collisions at the end of its range. Depending on the masses of host and impurity atoms as well as binding parameters of the host lattice, a probability can be calculated⁴⁰ that in the last collision the implanted atom displaces a host atom and is left with insufficient energy to leave the relative potential minimum at the substitutional lattice site. Thus even if an impurity energetically prefers an interstitial lattice site, this process can artificially increase the substitutional fraction of implanted atoms substantially. In the beryllium host investigated here, such end of range replacement collisions are kinematically impossible⁴⁰ for nearly all implanted elements. This is a direct consequence of the low mass of Be relative to the implanted atom.

The second source of disturbance in implantation processes is the creation of lattice defects. Lattice strain around an impurity atom of different size than the host atoms or electrostatic fields around one of different valence can act to attract mobile lattice defects. This trapping of defects at the impurity can destroy the correlation of the impurity site with the undisturbed host lattice, thus leading to a random result in a channeling study. In Be we expect this effect is minimized for a combination of reasons. After heavy ions slow to the point where a maximum energy-transfer collision cannot displace a Be atom from its site, it still has sufficient energy to travel a few lattice constants before stopping. Thus, it will not be stopped directly at or next to a vacancy it created itself. Also, the low mass of Be guarantees that the spatial density of defects in the collision cascade is low due to the long range of primary knock-ons. Finally, the mobility of vacancies, which are the primary defect at the core of the collision cascade, is low at room temperature with stage-III annealing occurring at ~ 350 K.

Thus we have reason to believe that the influence of ballistic aspects of the implantation process itself is smaller for the results we have presented above than

for those of previously studied analogous systems. We might therefore expect conventional metallurgical criteria to apply to some extent to this data. Indeed, we find that those elements known to show some, albeit small, solubility in Be, implant substitutionally. In addition, reportedly²² insoluble elements such as Zn (Ref. 14) and Os (Ref. 13) also find substitutional sites. So following the ideas of deWaard and Feldman⁴ and of Sood and Dearnaley,⁸ we display our lattice-location results on a Darken-Gurry plot⁵ in Fig. 15. A rough separation of substitutional and/or soluble cases from interstitial cases is clearly seen to be based mainly on atomic size with the interstitial impurities being the larger. This is an encouraging result in that it confirms the potential utility of such a parameterized display to systematize our results.

The separation in Fig. 15 is however not a clean one. The dashed line in the figure results from an attempt to topologically separate the substitutional and interstitial cases into two nonreentrant regions. Clearly the case of V vs Zn and to some extent of W and Mo vs Ag make this separation impossible. In addition, the tetrahedral and octahedral-like results are not well separated, mainly because of the relative positions of the Ga, Cd, and In points. Nevertheless, considering the fact that the Darken-Gurry parameterization coupled with the Hume-Rothery rules is no

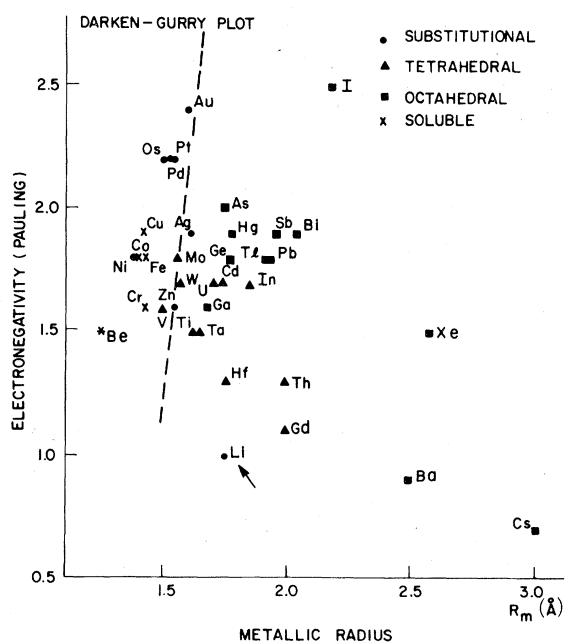


FIG. 15. Darken-Gurry plot for elements localized in Be after implantation. The ordinate is Pauling the electronegativity of the element and the abscissa is the metallic radius derived from the molar volume. The dashed line shows the approximate division of substitutional and interstitial impurities.

more than 75% accurate^{7,41} when applied to conventional equilibrium systems, it appears to work with the same success ratio for our data.

An alternative parameterization scheme which has >95% demonstrated success in predicting signs of the heats of formation of several hundred binary alloys is available to apply to our data. This scheme, devised recently by Miedema and co-workers,⁴² replaces the two variables of the Darken-Gurry plot with ϕ^* , related to the electronic work function of the elemental metal, and n_{ws} , proportional to the electron density at the boundary of the Wigner-Seitz cell in the metal. In Fig. 16 these parameters are used to systematize the results of this lattice-location study. This Miedema plot shows a clear separation between elements on substitutional, tetrahedral, and octahedral sites in the beryllium host. The high degree of success of the Miedema parameters implies that they are not only measures of the energies involved in the formation of equilibrium alloys but additionally contain information about the energies involved in the local lattice relaxation around the implanted impurity atom.

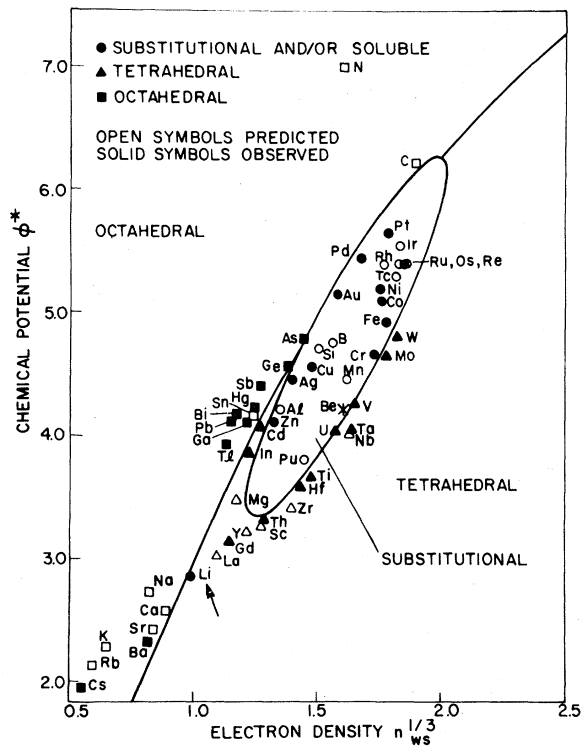


FIG. 16. Miedema plot for all tabulated elements (Ref. 42), with slight modifications of the coordinates of Al, Ga, In, Cd, and Ca (Ref. 43). The full lines separate the substitutional, tetrahedral, and octahedral domains as explained in the text.

The curves separating the substitutional, tetrahedral, and octahedral domains are obtained by using the Miedema coordinates of the implanted elements relative to Be in a modified Landau-Ginsburg expansion of the site energy differences for each element, a procedure explained in detail in Refs. 17 and 43. An interesting conclusion might be drawn from the fact that Be itself lies nearly on the border between the substitutional and the tetrahedral domains. It could indicate that a Be self-interstitial would prefer the tetrahedral interstitial space in the Be lattice.

The data point in Fig. 16 corresponding to the Li impurity clearly violates the excellent topological separation achieved for the other data. It is clear in this case¹⁶ that rather than being nearly independent of the ballistic artifacts of implantation the final substitutional site for Li is completely determined by ballistic effects. This arises from the combined influence of three factors: (a) Li is comparable in mass to Be, (b) Li diffuses as an interstitial in Be far faster than self-interstitials do, and (c) there exists an attractive interaction between a Li interstitial and a Be vacancy. The ballistics of the Li slowing down process guarantees the presence of a vacancy nearby the stopped Li which then diffuses to and is trapped at the vacant site. Thus one should not expect the metallurgical criteria embodied in Fig. 16 to apply. Similarly, the inconclusive results for other light impurities in Be, which were discussed briefly in Sec. III D, can be attributed to defect interactions. In these cases we have no information on impurity mobility or on the strength and sign of interactions with nearby vacancies. Thus, unlike the Li case, the exact process by which a site is chosen and indeed what site is likely is not known.

VI. CONCLUSIONS

This series of experiments is believed to yield the first set of true metallurgical site preference data upon implantation in a host metal, uninfluenced by artifacts of the implantation process itself. In view of this, the success of the Miedema scheme, especially its superiority to the Darken-Gurry plot, indicates that in the elemental parameters ϕ^* and n_{ws} information about short-range isotropic forces which predominate in most intermetallic alloys are implicitly contained. Probably even a higher degree of reliability of the Miedema plot could be reached if directional forces in the host lattice are included as suggested by Chelikowsky.⁴³

Apart from observed systematics, the present investigation suggests further experimental work. It would be interesting to study the detailed behavior of the implants in Be upon annealing as well as to ex-

tend such studies to other hosts. Here in view of different, usually lower lying, annealing stages it may be necessary to perform the implantation at low temperatures and subsequently determine the lattice location without an intermediate warm-up which would give lattice defects a chance to destroy unique primary configurations. On the other hand, from the standpoint of radiation-damage studies, such effects could contribute to the understanding of impurity-defect interactions. Initial experiments of this type have been performed by Swanson *et al.*³⁹ on substitutional systems after the production of defects by low-temperature ion bombardment. It was found that at the temperatures where host interstitials became mobile they were trapped at the substitutional impurities and formed so-called mixed dumbbells. Similar experiments on Be are in progress and may lead to a more detailed description of the local interstitial configuration.

ACKNOWLEDGMENTS

We would like to thank M. F. Robbins, W. M. Augustyniak, and W. F. Flood for help with computer programming, accelerator operation, and sample preparation. For useful discussions at various stages of this work, we are indebted to J. M. Poate, L. C. Feldman, W. D. Wilson, S. M. Myers, S. T. Picraux, R. Taylor, M. S. Duesbury, J. H. Barrett, J. R. Chelikowsky, and J. C. Phillips. We are indebted to R. B. Alexander and P. T. Callaghan for advice in computer analysis of channeling data and for supplying copies of their programs. One of us (R.V.) is grateful to Bell Laboratories for the hospitality shown during this work and acknowledges the support of a NATO postdoctoral fellowship. The extensive numerical calculations were performed on the Honeywell 6000 computer at Bell Laboratories and on the IBM 370/168 of the Universität Bonn.

*Resident visitor at Bell Laboratories. Present address: Institut für Strahlen- und Kernphysik d. Univ. Bonn, 5300 Bonn, West Germany.

¹See, e.g., G. Dearnaley, *Mater. Eng. Appl.* **1**, 28 (1978).

²J. M. Poate, *J. Vac. Sci. Technol.* **15**, 1636 (1978).

³S. T. Picraux, in *New Uses of Ion Accelerators*, edited by J. F. Ziegler (Plenum, New York, 1975), p. 229 (see tables on pp. 268–272).

⁴H. deWaard and L. C. Feldman, in *Applications of Ion Beams to Metals*, edited by S. T. Picraux, E. P. EerNisse, and F. L. Vook (Plenum, New York, 1974), p. 317.

⁵L. S. Darken and R. W. Gurry, *Physical Chemistry of Metals* (McGraw-Hill, New York, 1953).

⁶W. Hume-Rothery, R. E. Smallman, and C. Haworth, *The Structure of Metals and Alloys*, 5th ed. (Institute of Metals, London, 1969).

⁷J. T. Waber, L. Gscheidner, A. C. Lorrison, and M. Prince, *Trans. Met. Soc. AIME* **227**, 717 (1963).

⁸D. K. Sood and G. Dearnaley, in *Applications of Ion Beams to Materials*, edited by G. Carter, J. S. Colligon, and W. A. Grant, *Inst. Phys. Conf. Ser. No. 28* (IOP, London, 1976), p. 196; D. K. Sood, *Phys. Lett. A* **68**, 469 (1978); D. K. Sood and G. Dearnaley, *Radiat. Eff.* (in press).

⁹E. N. Kaufmann, P. Raghavan, R. S. Raghavan, E. J. Ansaldo, and R. A. Naumann, *Phys. Rev. Lett.* **34**, 1558 (1975).

¹⁰K. Krien, J. C. Soares, K. Freitag, R. Tischler, G. N. Rao, H. G. Müller, E. N. Kaufmann, A. Hanser, and B. Feurer, *Phys. Rev. B* **14**, 4782 (1976).

¹¹K. Krien, H. Saitovich, K. Freitag, F. Reuschenbach, J. C. Soares, and E. N. Kaufmann, *Hyper. Inter.* **4**, 549 (1978).

¹²B. Perscheid, H. W. Geyer, K. Krien, K. Freitag, J. C. Soares, E. N. Kaufmann, and R. Vianden, *Hyper. Inter.* **4**, 554 (1978).

¹³E. N. Kaufmann and R. Vianden, *Phys. Rev. Lett.* **38**, 1290 (1977).

¹⁴E. N. Kaufmann, *Phys. Lett. A* **61**, 479 (1977).

¹⁵R. Vianden and E. N. Kaufmann, *Nucl. Instrum. Methods* **149**, 393 (1978).

¹⁶E. N. Kaufmann, R. Vianden, T. E. Jackman, J. R. MacDonald, and L. G. Haggmark, *J. Phys. F* **9**, L23 (1979); M. S. Duesbery and R. Taylor, *ibid.* **9**, L19 (1979).

¹⁷E. N. Kaufmann, R. Vianden, J. R. Chelikowsky, and J. C. Phillips, *Phys. Rev. Lett.* **39**, 1671 (1977).

¹⁸J. A. Davies, in *Channeling*, edited by D. V. Morgan (Wiley, London, 1973).

¹⁹Franklin Inst. Research Laboratories, Philadelphia, Pa.

²⁰H. E. Schiott, *Radiat. Eff.* **6**, 107 (1970).

²¹M. Hansen, *Constitution of Binary Alloys* (McGraw-Hill, New York, 1958).

²²R. P. Elliott, *Constitution of Binary Alloys. 1st Suppl.* (McGraw-Hill, New York, 1965).

²³F. A. Shunk, *Constitution of Binary Alloys. 2nd Supplement* (McGraw-Hill, New York, 1969).

²⁴A. Kaufmann, P. Gordon, and D. N. Lillie, *Trans. Am. Soc. Met.* **42**, 801 (1950).

²⁵W. G. Moffatt, *The Handbook of Binary Phase Diagrams* (General Electric Company, Schenectady, N.Y., 1977).

²⁶W. B. Pearson, *Lattice Spacings and Structures of Metals and Alloys* (Pergamon, New York, 1958).

²⁷S. M. Myers and R. A. Langley, *J. Appl. Phys.* **46**, 1034 (1975).

²⁸R. A. Boie and K. R. Wildenauer, *Nucl. Instrum. Methods* **149**, 749 (1978).

²⁹P. Raghavan, R. S. Raghavan, E. N. Kaufmann, E. J. Ansaldo, and R. A. Naumann, in *International Conference on Hyperfine Interactions Studied in Nuclear Reactions and Decay*, edited by E. Karlson and E. Wäppling (Uppsala, Sweden, 1974), p. 42.

³⁰T. E. Jackman, J. R. MacDonald, R. Vianden, and E. N. Kaufman (unpublished).

³¹E. N. Kaufmann (unpublished).

³²J. Lindhard, *Dan. Vidensk. Selsk. Mat.-Fys. Medd.* **34**, No. 14 (1965).

³³R. B. Alexander, P. T. Callaghan, and J. M. Poate, *Phys. Rev. B* **9**, 3022 (1974).

³⁴E. N. Kaufmann, *Phys. Rev. B* **17**, 1024 (1978).

³⁵D. V. Morgan and D. VanVliet, AERE-Report, AERE-

- R6283 (2nd ed.), Harwell, 1970 (unpublished).
- ³⁶D. S. Gemmel, *Rev. Mod. Phys.* 46, 129 (1974).
- ³⁷*American Institute of Physics Handbook*, 3rd ed. (McGraw-Hill, New York, 1972), pp. 4–115.
- ³⁸R. B. Alexander and R. J. Petty, *Phys. Rev. B* 18, 981 (1978).
- ³⁹M. L. Swanson, L. M. Howe, A. F. Quenneville, and J. F. Watters, *J. Nucl. Mater.* 67, 42 (1977); M. L. Swanson, L. M. Howe, and A. F. Quenneville, *Radiat. Eff.* 28, 205 (1976).
- ⁴⁰D. K. Brice, in *Applications of Ion Beams to Materials*, edited by G. Carter *et al.*, *Inst. of Phys. Conf. Ser. No. 28* (IOP, London, 1976), p. 334.
- ⁴¹J. R. Chelikowsky and J. C. Phillips, *Phys. Rev. B* 17, 2453 (1978).
- ⁴²A. R. Miedema, *J. Less-Common Met.* 32, 117 (1973); A. R. Miedema, F. R. de Boer, and P. F. de Chatel, *J. Phys. F* 3, 1558 (1973); A. R. Miedema, R. Boom, and F. R. de Boer, *J. Less-Common Met.* 41, 283 (1975); R. Boom, F. R. de Boer, and A. R. Miedema, *J. Less-Common Met.* 46, 271 (1976); A. R. Miedema, *Phillips Tech. Rev.* 36, 217 (1976).
- ⁴³J. R. Chelikowsky, *Phys. Rev. B* 19, 686 (1979).
- ⁴⁴W. Hume-Rothery, *Institute of Metals Monograph No. 26* (Institute of Metals, London, 1966), p. 50.